Peierls instability and optical response in the one–dimensional half–filled Holstein model of spinless fermions

A. Weiße and H. Fehske

Physikalisches Institut, Universität Bayreuth, D–95440 Bayreuth, Germany

(Bayreuth, 22 June 1998)

Abstract

The effects of quantum lattice fluctuations on the Peierls transition are studied within the one–dimensional Holstein molecular crystal model by means of exact diagonalization methods. Applying a very efficient variational Lanczos technique, the ground–state phase diagram is obtained in excellent agreement with predictions of recent density matrix renormalization group calculations. The transition to the charge–density–wave regime is signaled by a strong increase in the charge structure factor. In the metallic regime, the non–universal Luttinger liquid parameters (charge velocity and coupling constant) are deduced from a finite–size scaling analysis. The variational results are supported by a complete numerical solution of the quantum phonon Holstein model on small clusters, which is based on a well–controlled phonon Hilbert space truncation procedure. The metallic and charge–density–wave phases are characterized by significant differences in the calculated optical absorption spectra.

PACS number(s): 71.38.+i, 71.45.Lr, 72.10.Di

I. INTRODUCTION

Many quasi one–dimensional (1D) materials, such as the organic conjugated polymers [e.g., $(CH)_x$] and charge transfer salts [e.g., TTF(TCNQ)] or the inorganic blue bronzes [e.g., $K_{0.3}MoO_3$] and MX–chains [1], undergo a Peierls instability in the half–filled band case at temperatures between 50 K and 250 K, driven by the electron–phonon (EP) interaction [2]. Most theoretical studies of these systems concentrate on the 1D SSH [3] and Holstein [4] models, where the phonons interact with the electrons by modifying the electron hopping matrix element and on–site potential, respectively. Frequently the lattice degrees of freedom were treated classically. However, it has been argued that for most quasi–1D systems the lattice zero–point motion is comparable to the Peierls lattice distortion, which makes the rigid lattice approximation questionable [5]. Although the problem, whether the dimerized ground state survives the quantum phonon fluctuations, has been addressed by several numerical [6–8] and analytical [9–11] approaches, it has to date resisted a complete theoretical solution. Moreover, lattice dynamical (quantum phonon) effects should be included in any theoretical analysis of the extraordinary transport and optical phenomena observed in Peierls–distorted systems [12,13]. The discussion of optical properties, e.g., of the optical absorption, poses, however, an extremely complicated many–body problem that cannot be solved analytically without further approximations [14,15]. Perhaps, at present, the most reliable results for models of electrons strongly interacting with quantum phonons come from finite–cluster calculations supplemented by a careful finite–size analysis.

Encouraged by this situation, in this work we present a purely numerical (exact diagonalization) study of the 1D spinless fermion Holstein model [16], with a view to understanding the effect of quantum lattice fluctuations on the Peierls dimerization and optical absorption spectra in both the metallic [Luttinger liquid (LL)] and insulating [charge–density–wave (CDW)] phases. In a particle–hole symmetric notation the Holstein Hamiltonian reads

$$\mathcal{H} = -t \sum_i (c_i^\dagger c_{i+1} + c_{i+1}^\dagger c_i) - \sqrt{\varepsilon_p \hbar\omega_0} \sum_i (b_i^\dagger + b_i)\,(n_i - \tfrac{1}{2}) + \hbar\omega_0 \sum_i (b_i^\dagger b_i + \tfrac{1}{2})\,, \qquad (1)$$

where $c_i^{[\dagger]}$ ($b_i^{[\dagger]}$) are the electron (phonon) annihilation [creation] operators, and $n_i = c_i^\dagger c_i$. In Eq. (1), the free–electron transfer amplitude t is restricted to nearest–neighbour hopping, a dispersionsless Einstein phonon $\omega(q) = \omega_0$ is coupled to the local electron density, and the phonons are treated within harmonic approximation. In the atomic limit ($t = 0$), ε_p gives the well–known Lang–Firsov polaron binding energy. Rescaling $\mathcal{H} \rightarrow \mathcal{H}/t$ and measuring all energies in units of t, it is convenient to introduce the adiabaticity parameter $\alpha = \hbar\omega_0/t$ and two dimensionless EP coupling constants, $\lambda = \varepsilon_p/2t$ and $g = \sqrt{\varepsilon_p/\hbar\omega_0}$, in order to characterize the weak ($\lambda \ll 1$) and strong coupling ($\lambda \gg 1$ *and* $g \gg 1$) situations in the adiabatic ($\alpha \ll 1$) and anti–adiabatic ($\alpha \gg 1$) regimes. For the single–carrier case, the Holstein Hamiltonian was extensively studied in the context of the polaron problem. A practically complete numerical solution, including ground state and spectral properties, is now available from ED (exact diagonalization) and DMRG (density matrix renormalization group) calculations [17–19]. At half–filling, a number of different analytical and numerical methods, including strong coupling expansions [7], variational approaches [20] and renormalization group arguments [21], as well as world–line quantum Monte Carlo (WL QMC) [7], Green's function Monte Carlo (GF MC) [8] and DMRG techniques [22], have been used to determine the phase boundary between metallic and insulating behaviour.

In this paper, we follow our strategy pursued in recent work on the self–trapping problem in the single–electron Holstein model [23], and apply two different numerical methods: (i) a complete exact diagonalization (ED) of the Holstein model preserving the full dynamics and quantum nature of phonons and (ii) a variational Lanczos scheme based on the inhomogeneous modified variational Lang–Firsov transformation (IMVLF) [24]. It is natural for the first method to be limited to rather small clusters (with N sites) and moderate EP coupling strengths ($\lambda,\ g$), mainly due to the necessity of a phonon Hilbert space truncation (retaining at most M phonons; for details of the numerical method see Ref. [25]). By combining ED with Chebyshev recursion and maximum entropy methods [26,25], we are able to discuss the dynamical properties of the spinless fermion Hol-

stein model, such as the optical conductivity (see Sec. IV). On the other hand, using the second method, we can study the ground–state properties of fairly large systems (Sec. II), which enables us to carry out a finite–size scaling (cf. Sec. III). Within the IMVLF–Lanczos approach, we treat the phonon subsystem by performing first of all a canonical transformation, $\tilde{\mathcal{H}} = \mathcal{U}^\dagger \mathcal{H} \mathcal{U}$, $\mathcal{U} = \mathrm{e}^{-\mathcal{S}_1(\Delta_i)}\, \mathrm{e}^{-\mathcal{S}_2(\gamma)}\, \mathrm{e}^{-\mathcal{S}_3(\tau)}$, where $\mathcal{S}_1(\Delta_i) = -\frac{1}{2g\alpha} \sum_i \Delta_i (b_i^\dagger - b_i)$, $\mathcal{S}_2(\bar{\gamma}, \gamma) = -g \sum_i (b_i^\dagger - b_i)\, (\bar{\gamma} + \gamma n_i)$, and $\mathcal{S}_3(\tau) = \frac{1}{2} \ln \tau \sum_i (b_i^\dagger b_i^\dagger - b_i b_i)$ are designed to describe static displacement field (Δ_i), non–adiabatic polaron ($\gamma, \bar{\gamma}$), and squeezing (τ) effects, respectively. Next, we approximate the eigenstates $|\tilde{\Psi}\rangle$ of the transformed Hamiltonian by the variational product states $|\tilde{\Psi}_V\rangle = |\tilde{\Psi}_{ph}\rangle \otimes |\tilde{\Psi}_{el}\rangle$ and average $\tilde{\mathcal{H}}$ over the phonon vacuum, $\bar{\mathcal{H}} \equiv \langle \tilde{\Psi}_{ph}^0 | \tilde{\mathcal{H}} | \tilde{\Psi}_{ph}^0 \rangle$, which leads to an effective electronic Hamiltonian

$$\begin{aligned} \bar{\mathcal{H}} = {} & g^2 \alpha (\bar{\gamma^2} + \bar{\gamma}) N \, + \, g^2 \alpha [\gamma^2 - \gamma + 2\bar{\gamma}(\gamma - 1)] \sum_i n_i \, - \, \mathrm{e}^{-g^2 \gamma^2 \tau^2} \sum_i (c_i^\dagger c_{i+1} + c_{i+1}^\dagger c_i) \\ & - (1 - \gamma) \sum_i \Delta_i \, (n_i - \tfrac{1}{2}) \, + \eta \sum_i \Delta_i \, + \, \frac{\alpha N}{4} (\tau^2 + \tau^{-2}) \, + \, \frac{1}{4 g^2 \alpha} \sum_i \Delta_i^2 \, . \end{aligned} \tag{2}$$

Here η is a Lagrange multiplier ensuring the constraint $\sum_i \Delta_i = 0$. Employing the Hellmann–Feynman theorem, the $N + 3$ variational parameters are obtained by iteratively solving the extremal equations for the corresponding energy functional $\bar{E}_0(\{\Delta_i\}, \bar{\gamma}, \gamma, \tau^2)$ in combination with the Lanczos recursion algorithm.

II. PHASE DIAGRAM

Previous results for the ground–state phase diagram of the Holstein model at half–filling obtained by WL QMC [7] and GF MC [8] simulations showed significant discrepancies in the region of small α ($0 < \alpha \lesssim 1$). Only very recently Bursill et al. [22] provided more reliable information from level crossings in their DMRG data. Applying, in a first step, our variational Lanczos scheme, we consider the effective model (2) on chains of even length with up to 16 sites and periodic (antiperiodic) boundary conditions if there is an odd (even) number of fermions in the system. To elude the problem of trapping in metastable minima of the energy functional $\bar{E}_0$, we start the variational Lanczos iteration with different initial

configurations $\{\Delta_i, \bar{\gamma}, \gamma, \tau^2\}$, close to the metallic or the dimerized phase. As one might expect, in the dimerized phase the iteration always converges to a ground–state with staggered dimerization $\Delta_i = \Delta(-1)^i$, while in the metallic phase $\Delta_i = 0$. Thus, at half–filling, our inhomogeneous variational wave function becomes exactly the staggered (SMVLF) one used in Ref. [20], and the effective Hamiltonian $\bar{\mathcal{H}}(\Delta, \gamma, \tau^2)$ can be solved easily, also for the infinite system. However, the phase diagram given in [20] for the infinite system is only tentative, and for small α the determination of g_c is not clear. Moreover the infinite system is never really gapless within the variational approach, because Δ remains nonzero, although it becomes very small for weak EP coupling. This situation changes as soon as the system is finite. The dimerization Δ then switches from zero to a finite value at a critical coupling $g_c(\alpha, N)$, where g_c is nearly independend from the system–size N for large α ($\alpha \gtrsim 1$), but decreases with N for small α.

Proceeding this way we get the IMVLF transition lines $g_c(\alpha, N)$ depicted in Fig. 1. Most notably we found that the IMVLF phase boundary, separating metallic (LL) and insulating (CDW) phases, in the whole parameter regime, agrees surprisingly well with the very recent DMRG results [22] (open squares). Also in the phase diagram are the transition points obtained by WL QMC [7] and GF MC [8].

In a second step, performing exact diagonalizations of the full Hamiltonian for systems with 6 and 10 sites and up to 30 phonons, we want to demonstrate that the phase boundary determined from the effective model (2) is consistent with what is obtained for the quantum phonon Holstein model (1). To this end, we have calculated the static charge structure factor,

$$\chi(\pi) = \frac{1}{N} \sum_{i,j} \mathrm{e}^{i\pi(R_i - R_j)} \langle n_i n_j \rangle \,, \tag{3}$$

shown in Fig. 2 as a function of g at low (a), intermediate (b), and high (c) phonon frequencies for both, the variational and the exact solution. Increasing the EP coupling at fixed phonon frequency, the smooth variation of $\chi(\pi)$ in the metallic phase is followed by a strong enhancement at about $g_c^{(\mathrm{IMVLF})}$, unambiguously indicating the formation of a CDW.

The discontinuous jump–like behaviour of $\chi^{(\mathrm{IMVLF})}(\pi)$ at g_c is an apparent shortcoming of the variational approach. This resolves also the open question in [20], whether the two–minimum structure of the variational solution at large α is an artifact. For $\alpha \to 0$ and $N \to \infty$, where the IMVLF approach becomes exact, we found a continuous crossover in $\chi^{(\mathrm{IMVLF})}(\pi)$ as well.

Obviously, in the CDW–like phase, a larger number of phonons (M) is required to achieve a satisfactory convergence of the ED data (see Fig. 2 (b)). Furthermore, it is interesting to compare the behaviour of the kinetic energy $\langle E_{kin} \rangle$, given by the average of the first term of (1), in the adiabatic, non–adiabatic and anti–adiabatic regimes (see insets). For the adiabatic case, the kinetic energy is only weakly reduced from its noninteracting value ($\langle E_{kin} \rangle = -4$) in the metallic phase. By contrast, in the anti-adiabatic regime, we observe a strong reduction of $\langle E_{kin} \rangle$, which can be attributed to the formation of a strongly correlated polaronic metal *below* the CDW transition point.

Coming back to the phase diagram, in the *adiabatic regime*, our results seem to confirm that there is no long–range order for sufficiently small EP coupling, which is consistent with the predictions of Refs. [27,8]. At $\alpha = 0$, the critical coupling converges to zero, as expected for the adiabatic Hamiltonian ($M \to \infty$; $\gamma = 0$, $\tau^2 = 1$). In the regime $0 < \alpha \lesssim 1$, however, the precise determination of g_c is somewhat difficult. Maybe the discrepancy between the predictions of IMVLF, GF MC, DMRG on one side and WL MC on the other side, of how the critical λ_c scales to zero with $\alpha \to 0$, results from this ambiguity.

In the strong–coupling *non–adiabatic regime* (g^2, $\lambda \gg 1$), the results of the different numerical approaches approximately agree. Also the analytical approach, giving the exactly soluble XXZ model [7,28] within second order perturbation theory (with respect to t)

$$H^{\mathrm{XXZ}} = \frac{N}{4}(2\alpha - g^2\alpha - V_2) - \mathrm{e}^{-g^2} \sum_i \left((S_i^+ S_{i+1}^- + S_i^- S_{i+1}^+) - V_2 \, \mathrm{e}^{g^2} S_i^z S_{i+1}^z \right) \tag{4}$$

with

$$V_n(\alpha, g^2) = \frac{2e^{-ng^2}}{\alpha} \sum_{s \neq 0} \frac{(ng^2)^s}{ss!} \,, \tag{5}$$

works very well. The (Kosterlitz-Thouless) phase transition line is given by the condition $V_2(\alpha, g^2)\mathrm{e}^{g^2}/2 = 1$ (dashed curve in Fig. 1). For $\alpha \to \infty$ (anti–adiabatic limit) there is no dimerization if λ is finite.

To get a feeling about the accuracy of the different analytical and numerical techniques, we have compared in Fig. 3 the ground–state energies at high phonon frequencies, where the small polaron approximation is justified. For the adiabaticity ratio $\alpha = 10$, used in Fig. 3, the transition to the CDW phase takes place at about $g_c \simeq 2$.

Restricting ourselves to the metallic phase, the ground–state energy of the XXZ model is easy to evaluate. It is (per site)

$$E_0^{\mathrm{XXZ}} = \frac{\alpha}{2} - \frac{g^2\alpha}{4} - \sin[\mu]\,\mathrm{e}^{-g^2}\int_{-\infty}^{\infty} dx \frac{\sinh[(\pi-\mu)x]}{\sinh[\pi x]\sinh[\mu x]} \tag{6}$$

with $\cos[\mu] = V_2\,\mathrm{e}^{g^2}/2$. Alternatively, calculating the polaron self–energy of the Holstein model (1) within standard second–order (Rayleigh–Schrödinger) strong–coupling perturbation theory (SCPT) and omitting the residual polaron interaction, the small polaron band dispersion becomes [18]

$$E_K^{\mathrm{SCPT}} = -\frac{g^2\alpha}{2} + V_2 - 2\mathrm{e}^{-g^2}\cos K - V_1\,\mathrm{e}^{-g^2}\cos 2K\,. \tag{7}$$

Then, for the half–filled band case, the ground–state energy (per site) takes the form

$$E_0^{\mathrm{SCPT}} = E_0^{(1)} + \frac{V_2}{2}\,, \tag{8}$$

where the (first–order) polaron ground–state energy,

$$E_0^{(1)} = \frac{\alpha}{2} - \frac{g^2\alpha}{4} - 2\mathrm{e}^{-g^2}/\pi\,, \tag{9}$$

can be obtained from (2) by setting $\Delta_i = 0$, $\gamma = 1$, $\bar{\gamma} = -1/2$, and $\tau^2 = 1$.

Both E_0^{XXZ} and E_0^{SCPT} are also depicted in Fig. 3, and in order to visualize the higher–order corrections we have shifted all energies by the standard small polaron term $E_0^{(1)}$. First of all we see that the higher–order corrections, originated by the residual polaron–phonon interaction, are most important at intermediate couplings $g \simeq 1$, where the polaron band

structure significantly deviates from a rescaled cosine tight–binding band [18]. As already mentioned above, the IMVLF–Lanczos results, extrapolated to $N = \infty$, coincide with the variational SMVLF solution [20], but give higher ground–state energies than the XXZ model in the intermediate–to–strong coupling regime. This is because the non–adiabatic polaron effects are only included to the lowest order of approximation (remind that the model (2) was obtained performing the average over the zero–phonon state). Including second order corrections by SCPT, we found a much better agreement with the exact data (full circles). Notice the substantial lowering of the energy with respect to the first order result at large EP couplings [$g = 2$ implies $\lambda = 20$ (!)], which results from the momentum independent shift in the kinetic energy [19,29]. As expected, the finite–size effects due to the lattice discreteness are most pronounced in the weak–coupling regime.

III. LUTTINGER LIQUID PARAMETERS

According to Haldane's Luttinger liquid conjecture [30], 1D gapless systems of interacting fermions should belong to the same universality class as the Tomonaga-Luttinger model. As stated above, the Holstein system is gapless for small enough coupling g. Thus it is obvious to prove, following the lines of approach to the problem by McKenzie et al. [8], whether our IMVLF–Lanczos data shows a finite–size scaling like a Luttinger liquid.

For a LL of spinless fermions, the ground–state energy $E_0(N)$ of a finite system of N sites scales to leading order as [31]

$$\frac{E_0(N)}{N} = \epsilon_\infty - \frac{\pi u_\rho}{6N^2}\,, \tag{10}$$

where ϵ_∞ denotes the ground–state energy per site for the infinite system and u_ρ is the velocity of the charge excitations. If $E_{\pm1}(N)$ is the ground–state energy with ±1 fermions away from half filling, to leading order the scaling should be

$$E_{\pm1}(N) - E_0(N) = \frac{\pi u_\rho}{2K_\rho N}\,. \tag{11}$$

K_ρ is the renormalized effective coupling (stiffness) constant (for a more detailed discussion see Ref. [8]).

As becomes evident from Fig. 4, our IMVLF–Lanczos data match both scaling relations for all regimes of parameters α and g with great accuracy. Let us stress that the IMVLF–energies for $E_{\pm 1}(N)$ correspond to a inhomogeneous solution for the displacement fields Δ_i, which deviates from a uniform or staggered ordering, and therefore cannot be obtained within the simple SMVLF scheme [20].

In the plot of the LL parameters, Fig. 5, increasing error bars at the end of the curves indicate the phase transition to the CDW state. Here the scaling relations (10) and (11) no longer hold. Perhaps surprising, the velocity of charge excitations u_ρ, reflecting the behaviour of the kinetic energy (cf. Fig. 2 insets), agrees fairly well with the results of McKenzie et al. [8], while the coupling constant K_ρ is always bigger than one, indicating an attractive interaction. We believe this is an artifact of our variational treatment. For the XXZ model $K_\rho \to 1/2$, i.e. the phase transition is of infinite order [33] with a Kosterlitz–Thouless order parameter $\sim e^{-1/(g-g_c)}$. Note that the parameters u_ρ and K_ρ we show, are of course those for the effective Hamiltonian (2), which coincide with the parameters of the true Holstein model only more or less.

Unfortunately, extracting a similar scaling behaviour from our ED data seems to be extremely complicated, mainly because *two* finite–size dependences, those with respect to the system size N and maximum phonon number M, are mixed. Moreover, the memory limitations of the present day parallel computers impose severe restrictions on the lattice sizes ($N \leq 10$), that can be treated by ED with adequate accuracy.

IV. OPTICAL RESPONSE

One of the physical quantities which contains extremely valuable information about the low–energy excitations in polaronic metals and CDW systems is the optical conductivity, $\sigma(\omega)$, usually determined from reflectivity measurements. As will be shown in the following,

the optical absorption spectra of nearly free electrons, small polarons and CDW insulators differ essentially.

The real part of $\sigma(\omega)$ contains two contributions, the familiar (coherent) Drude part at $\omega = 0$ and a so–called "regular term", $\sigma^{reg}(\omega)$, due to finite–frequency dissipative optical transitions to excited quasiparticle states. In spectral representation ($T = 0$), the regular part takes the form [25,32]

$$\sigma^{reg}(\omega) = \sum_{m>0} \frac{|\langle\Psi_0|i\sum_j(c_j^\dagger c_{j+1} - c_{j+1}^\dagger c_j)|\Psi_m\rangle|^2}{E_m - E_0}\, \delta[\omega - (E_m - E_0)]\,, \tag{12}$$

where $\sigma^{reg}(\omega)$ is given in units of πe^2 and we have omitted an $1/N$ prefactor. In (12), the summation is taken over the complete set of eigenstates $|\Psi_m\rangle$ with excitation energies $\omega = (E_m - E_0)$ in the subspace of $N/2$ (spinless) fermions (half–filling). For the discussion of the optical properties it is useful to consider also the ω–integrated spectral weight function

$$\mathcal{S}^{reg}(\omega) = \int_0^\omega d\omega' \sigma^{reg}(\omega')\,. \tag{13}$$

The evaluation of dynamical correlation functions, such as (12), can be carried out by means of very efficient and numerically stable Chebyshev recursion and maximum entropy algorithms [26,25]. Nevertheless, due to the huge size of the Hilbert space in this EP model, we are currently restricted to a lattice size of 6 sites ($M = 30$; periodic boundary conditions) if we want to calculate the conductivity in a wide range of EP coupling strengths.

Typical optical absorption spectra for the 1D half–filled Holstein model of spinless fermions are given by Figs. 6, 7, and 8, in the metallic (a) and CDW (b) phases, at characteristic phonon frequencies corresponding to the adiabatic, intermediate, and anti–adiabatic regimes, respectively.

For *low phonon frequencies* ($\alpha \ll 1$) and weak EP couplings (see Fig. 6 a), the peak structure may be easily understood in connection with the non–interacting tight–binding band dispersion $E_K^{(0)} = -2\cos K$, where the allowed K values are $K = 0$, $\pm\pi/3$, $\pm 2\pi/3$, and π for a six site system. Obviously, we found the first transitions with non–negligible (electronic) spectral weight (cf. $S^{reg}(\omega)$) at frequencies that approximately correspond to

to the discrete free electron Bloch states of our finite system and its vibrational satellites. Accordingly the first and second group of excitations originate from transitions where the momentum of one electron is changed from $\pm\pi/3$ to $\pm 2\pi/3$ and $\pm\pi/3$ to $\pm\pi$, respectively. Note that in (12) an optical transition only takes place within the $K = 0$ sector ($|\Psi_0\rangle$ carries $K = 0$ for the half–filled band case). Thus a phonon with opposite momentum must be absorbed in order to ensure momentum conservation during a single–particle excitation process. Of course, in the Holstein model, K is the *total* momentum of the coupled EP system, and, at any $g > 0$, there is a finite overlap of the ground state with all the excited states belonging to the same K sector. The most relevant point is that in the metallic phase the absorption threshold should tend to zero as the number of sites increases, i.e., the low–energy (finite–size) gap vanishes.

The optical absorption spectrum in the strong EP coupling regime is quite different from that in the LL phase. It can be interpreted in terms of strong electron–phonon correlations and corroborates the CDW picture. For $g > g_c$ the electronic band structure is gapped (at the edge points $K = \pm\pi/2$), and we expect that now the low–energy gap feature, observed in Fig. 6 (b), survives in the thermodynamic limit $N \to \infty$. Unfortunately finite–size effects prevent a precise extraction of the CDW gap from our optical ED data. The broad optical absorption band found above this gap is produced by a single-particle excitation accompanied by multi–phonon absorptions and is basically related to the lowest unoccupied state of the upper band of the CDW insulator. The lineshape reflects the phonon distribution in the ground state (see Fig. 9). The most striking feature is the strong increase of the spectral weight contained in the incoherent part of optical conductivity. This becomes evident by comparing the magnitude of $S^{reg}(\infty)$ in the weak and strong coupling situations. Moreover, employing the f–sum rule for the optical conductivity [23] and taking into account the behaviour of the kinetic energy as function of g (see Fig. 3), we found that in the metallic and CDW phases nearly all the spectral weight is contained in the coherent (Drude) and incoherent (regular) part of Re $\sigma(\omega)$, respectively. That is, in the CDW state the transport is dominated by inelastic scattering processes.

In the *non–adiabatic region* $\alpha \simeq 1$, where the phonon frequency becomes comparable to the electronic bandwidth (level spacing), the situation is not much different (see Fig. 7). Again, in the weakly interacting case, the optical absorption can be understood in terms of electronic transitions within a tight–binding band and phonon satellites. Crossing the CDW transition point, a pronounced redistribution of spectral weight from the Drude to the regular part of $\sigma(\omega)$ is observed. As can be seen by comparing Figs. 6–8 and Fig. 9, the heights of the jumps in the ω–integrated conductivity, being directly related to the probability of the corresponding m–phonon absorption processes, give a measure of the weights of the m–phonon states in the ground state.

Finally, we consider the optical response in the *anti–adiabatic regime*. For weak interaction the picture remains the same as in the above adiabatic and intermediate cases (see Fig. 8). If we increase the EP coupling g, the electrons will be heavily dressed by the phonons (which now can follow the electron instantaneously) and the formation of less mobile small polarons takes place (cf. $\langle E_{kin}(g)\rangle$ and $u_\rho(g)$ shown in Fig. 3 (c) and Fig. 5 (a), respectively). As a consequence the coherent transport becomes strongly suppressed in the LL phase. Since the (renormalized) coherent bandwidth of the polaron band is rather small, the finite–size gaps in the band structure are reduced as well, and the CDW gap ($\Delta_{CDW} \sim 2\lambda$) may be identified with the optical absorption threshold. Again we found that in the CDW phase multi–phonon absorption processes dominate the optical response.

V. SUMMARY

In this paper we have studied the Peierls instability and the optical absorption in the half–filled spinless fermion Holstein model by means of finite–lattice diagonalizations. We have shown that the simple variational (IMVLF) Lanczos approach can be successfully used to determine the ground–state properties of the Holstein model, in particular the phase diagram. The calculation of the optical properties did require a complete diagonalization of the model, preserving the full dynamics of the phonons.

Our results confirm previous findings that at sufficiently weak electron–phonon (EP) interaction the system resides in a metallic (gapless) phase, described by two Luttinger liquid parameters. The renormalized charge velocity (u_ρ) and correlation exponent (K_ρ) were obtained from finite–size scaling relations, fulfilled with great accuracy. Increasing the EP coupling, the system undergoes a Peierls transition to an insulating (gaped) phase, reflected in a strong increase of the charge–density correlations with momentum π. The crossover between Luttinger liquid and charge–density–density (CDW) behaviour is found in good agreement with exact diagonalization and density matrix renormalization results for the quantum phonon model. In the non–adiabatic strong–coupling limit, where the charge carriers are polaronic, the IMVLF–Lanczos phase boundary lies close to the analytic findings for the XXZ (small polaron) model. The transition to the CDW state is accompanied by significant changes in the optical response of the system. Most notably seems to be the substantial spectral weight transfer from the Drude to the regular (incoherent) part of the optical conductivity, indicating the increasing importance of inelastic scattering processes in the CDW (Peierls distorted) regime.

The numerical results made clear that a dynamical treatment of the lattice degrees is necessary in the intermediate frequency and coupling region because the energy scales are not well separated. This should be a matter of relative importance modeling the inorganic spin Peierls materials [34], e.g. $CuGeO_3$, where the spin exchange interaction and the relevant phonon frequencies are of the same order. Indeed, applying our numerical techniques to a frustrated Heisenberg spin–$\frac{1}{2}$ chain with dynamic spin–phonon coupling shows that in the non–adiabatic regime the spin–Peierls transition takes place at about $g_c \sim 1$, which implies for $CuGeO_3$ a intermediate to strong coupling situation [35].

ACKNOWLEDGMENTS

The authors would like to thank G. Wellein and B. Bäuml for their support in the numerical work. We are particularly indebted to R. J. Bursill for putting his DMRG data

prior publication at our disposal, and to E. Jeckelmann for useful comments on the optical conductivity data. Calculations were performed at the LRZ München, HLRZ Jülich, and the HLR Stuttgart.

REFERENCES

[1] N. Tsuda, K. Nasu, A. Yanese, and K. Siratori, *Electronic Conduction in Oxides*, Springer–Verlag, (Berlin 1990); J.-P. Farges (Ed.), *Organic Conductors*, Marcel Dekker, (New York 1994).

[2] R. Peierls, *Quantum theory of solids*, Oxford University Press, (Oxford 1955).

[3] W. P. Su, J. R. Schrieffer, and A. J. Heeger, Phys. Rev. Lett. **42**, 1698 (1979).

[4] T. Holstein, Ann. Phys. **8**, 325 (1959); **8**, 343 (1959).

[5] R. H. McKenzie and J. W. Wilkins, Phys. Rev. Lett. **69**, 1085 (1992).

[6] E. Fradkin and J. E. Hirsch, Phys. Rev. B **27**, 1680 (1983).

[7] J. E. Hirsch and E. Fradkin, Phys. Rev. B **27**, 4302 (1983).

[8] R. H. McKenzie, C. J. Hamer, and D. W. Murray, Phys. Rev. B **53**, 9676 (1996).

[9] D. Schmeltzer, R. Zeyer, and W. Hanke, Phys. Rev. B **33**, 5141 (1986).

[10] G. C. Psaltakis and N. Papanicolaou, Solid State Commun. **66**, 87 (1988).

[11] C. Q. Wu, Q. F. Huang, and X. Sun, Phys. Rev. B **52**, R15683 (1995).

[12] G. Hutiray and J. S. (Eds.), *Charge Density Waves in Solids*, volume 217 of *Lecture Notes in Physics*, Springer, (Berlin 1985).

[13] L. Degiorgi et al., Phys. Rev. B **52**, 5603 (1995).

[14] H. Zheng and S. Y. Zhu, Phys. Rev. B **36**, 8736 (1996).

[15] F. Gebhard, K. Bott, M. Scheidler, P. Thomas, and S. W. Koch, Philos. Mag. B **75**, 1 (1997); **75**, 13 (1997); **75**, 47 (1997); J. Voit, Synth. Met. **27**, A41 (1988).

[16] The spinless fermion case may be of interest for strongly correlated electron systems (described, e.g., by the infinite–U limit of the Hubbard Holstein model), or, in view of the recently discovered inorganic spin Peierls compounds $GeCuO_3$ [M. Hase, I. Terasaki, and K. Uchinokura, Phys. Rev. Lett. **70**, 3651, (1993)], with respect to work on weakly coupled spin chains.

[17] J. Ranninger and U. Thibblin, Phys. Rev. B **45**, 7730 (1992); A. S. Alexandrov, V. V. Kabanov, and D. K. Ray, Phys. Rev. B **49**, 9915 (1994); G. Wellein and H. Fehske,

Phys. Rev. B **56**, 4513 (1997); M. Capone, W. Stephan, and M. Grilli, Phys. Rev. B **56**, 4484 (1997); J. M. Robin, Phys. Rev. B **56**, 13634 (1997); E. Jeckelmann and S. R. White, cond-mat/9710058.

[18] H. Fehske, J. Loos, and G. Wellein, Z. Phys. B **104**, 619 (1997).

[19] G. Wellein and H. Fehske, Phys. Rev. B **56**, 4513 (1997).

[20] H. Zheng, D. Feinberg, and M. Avignon, Phys. Rev. B **39**, 9405 (1989).

[21] L. G. Caron and C. Bourbonnais, Phys. Rev. B **29**, 4230 (1984).

[22] R. J. Bursill, R. H. McKenzie, and C. J. Hamer, cond-mat/9802215.

[23] G. Wellein and H. Fehske, Phys. Rev. B **xx**, xxx (1998).

[24] H. Fehske, H. Röder, G. Wellein, and A. Mistriotis, Phys. Rev. B **51**, 16582 (1995).

[25] B. Bäuml, G. Wellein, and H. Fehske, Phys. Rev. B **58**, xxx (1998).

[26] R. N. Silver, H. Röder, A. F. Voter, and J. D. Kress, J. of Comp. Phys. **124**, 115 (1996).

[27] G. Benfatto, G. Gallavotti, and J. L. Lebowitz, Helv. Phys. Acta **68**, 312 (1995).

[28] C. N. Yang and C. P. Yang, Phys. Rev. **150**, 321 (1966); Phys. Rev. **151**, 258 (1966).

[29] Y. A. Firsov and E. K. Kudinov, Fiz. Tverd. Tela **39**, xxx (1997).

[30] F. D. M. Haldane, Phys. Rev. Lett. **45**, 1358 (1980).

[31] J. Voit, Rep. Prog. Phys. **58**, 977 (1995).

[32] E. Dagotto, Rev. Mod. Phys. **66**,763 (1994).

[33] R. Shankar, Int. J. Mod. Phys. B **4**, 2371 (1990).

[34] As pointed out recently [L.G. Caron and S. Moukouri, Phys. Rev. Lett. **76**, 4050 (1996); H. Zheng, Phys. Rev. B **56**, 14414 (1997)], the XY model with spin–phonon coupling, which can be mapped onto the 1D Holstein model of spinless fermions, may be the simplest model containing the essential physics of a Spin–Peierls system.

[35] G. Wellein, H. Fehske, and A.P. Kampf, cond-mat/9804085; B. Büchner, H. Fehske, A.P. Kampf, and G. Wellein, cond-mat/9806002.

FIGURES

FIG. 1. Ground–state phase diagram of the 1D Holstein model of spinless fermions at half filling, showing the boundary between the Luttinger liquid (LL) and charge–density–wave (CDW) states. The IMVLF–Lanczos results are compared with the predictions of different analytical and numerical approaches.

FIG. 2. Charge structure factor $\chi(\pi)$ and kinetic energy $\langle E_{kin} \rangle$ (inset) as a function of the EP coupling g in the adiabatic (a), non–adiabatic (b), and anti–adiabatic (c) regimes.

FIG. 3. Dependence on the EP coupling of the ground state energy (shifted by $E_0^{(1)}$). The predictions of strong coupling expansions are confronted with IMVLF–Lanczos and ED results obtained for a six–site lattice at $\alpha = 10$.

FIG. 4. Finite–size scaling of the charge gap $E_{-1}(N) - E_0(N)$ and the ground state energy $E_0(N)$ (inset) for different values of g ($g^2 = 0.1$, 0.6, 1.1, 1.6, 2.0 from top to bottom) at $\alpha = 0.1$ (a), 1 (b), and 10 (c).

FIG. 5. LL parameters u_ρ [charge velocity (a)] and K_ρ [correlation exponent (b)] as a function of the EP coupling g. The dashed curves denote the corresponding results for the XXZ model at $\alpha = 10$.

FIG. 6. Regular part of the optical conductivity $\sigma^{reg}(\omega)$ (dotted line) and integrated spectral weight $S^{reg}(\omega)$ in the adiabatic weak (a) and strong (b) EP coupling regimes ($N = 6$, $M = 30$.

FIG. 7. The same as Fig. 6 but at $\alpha = 1$. The results in the LL and CDW regimes are shown an (a) and (b), respectively.

FIG. 8. Optical absorption in the anti–adiabatic regime ($\alpha = 10$) of the 1D half–filled Holstein model.

FIG. 9. Phonon–distribution function $|c^m|^2$, as defined in equation (A9) of [25], shown for the parameters used in FIG. 6–8.

Figure 1:

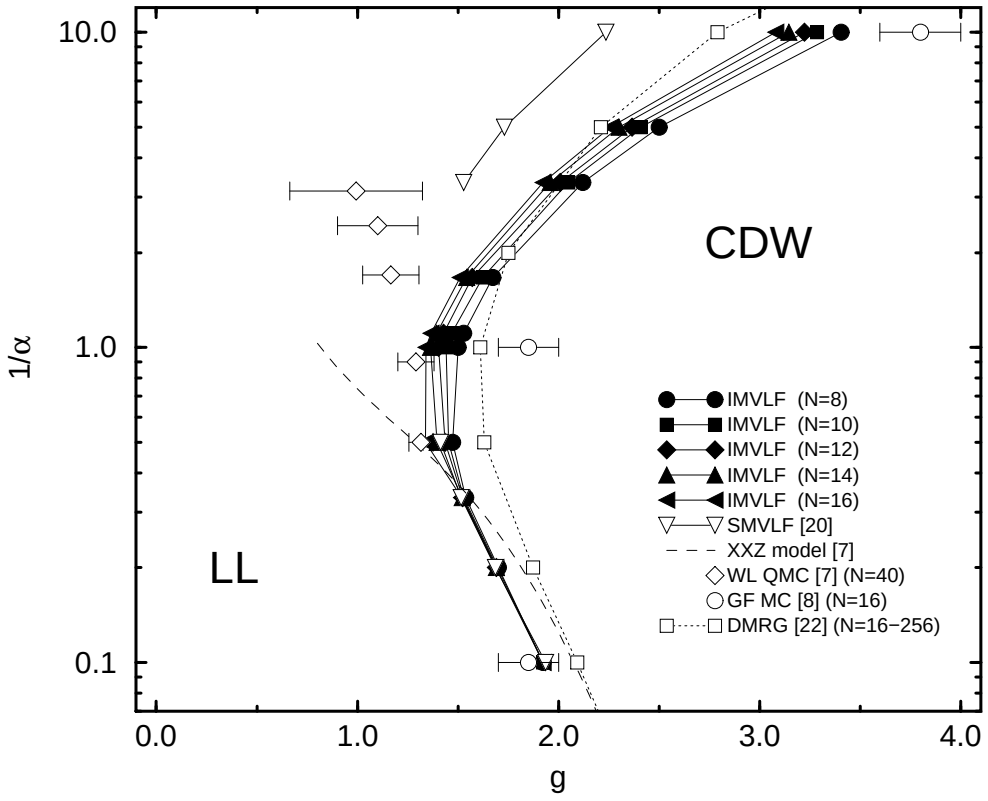
10.0
1.0
0.1
1/α
0.0
1.0
2.0
3.0
4.0
g
CDW
LL
IMVLF (N=8)
IMVLF (N=10)
IMVLF (N=12)
IMVLF (N=14)
IMVLF (N=16)
SMVLF [20]
XXZ model [7]
WL QMC [7] (N=40)
GF MC [8] (N=16)
DMRG [22] (N=16−256)

Figure 2:

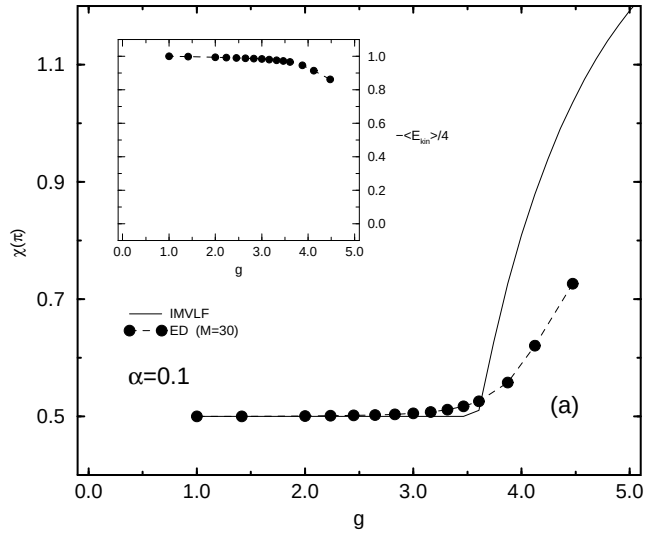
χ(π)
g
IMVLF
ED (M=30)
α=0.1
(a)
-<E_kin>/4

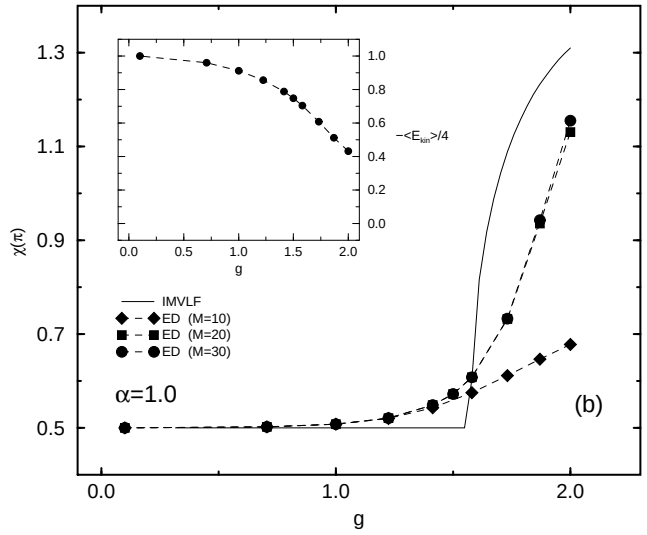
χ(π)
g
IMVLF
ED (M=10)
ED (M=20)
ED (M=30)
α=1.0
(b)
-<E_kin>/4

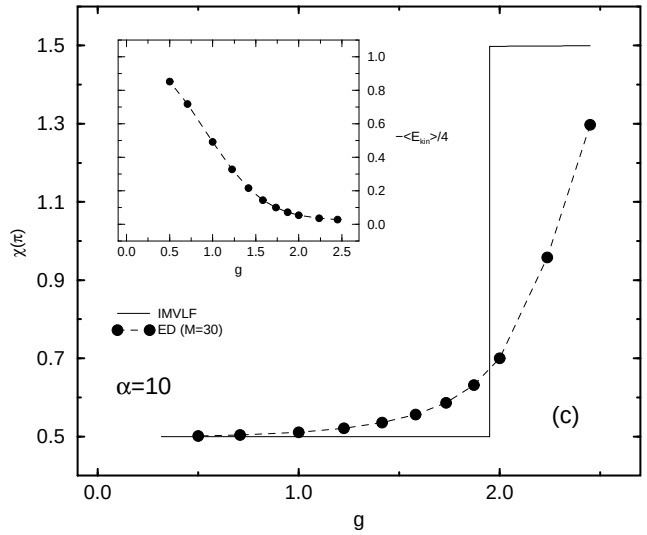
χ(π)
g
IMVLF
ED (M=30)
α=10
(c)
-<E_kin>/4

Figure 3:

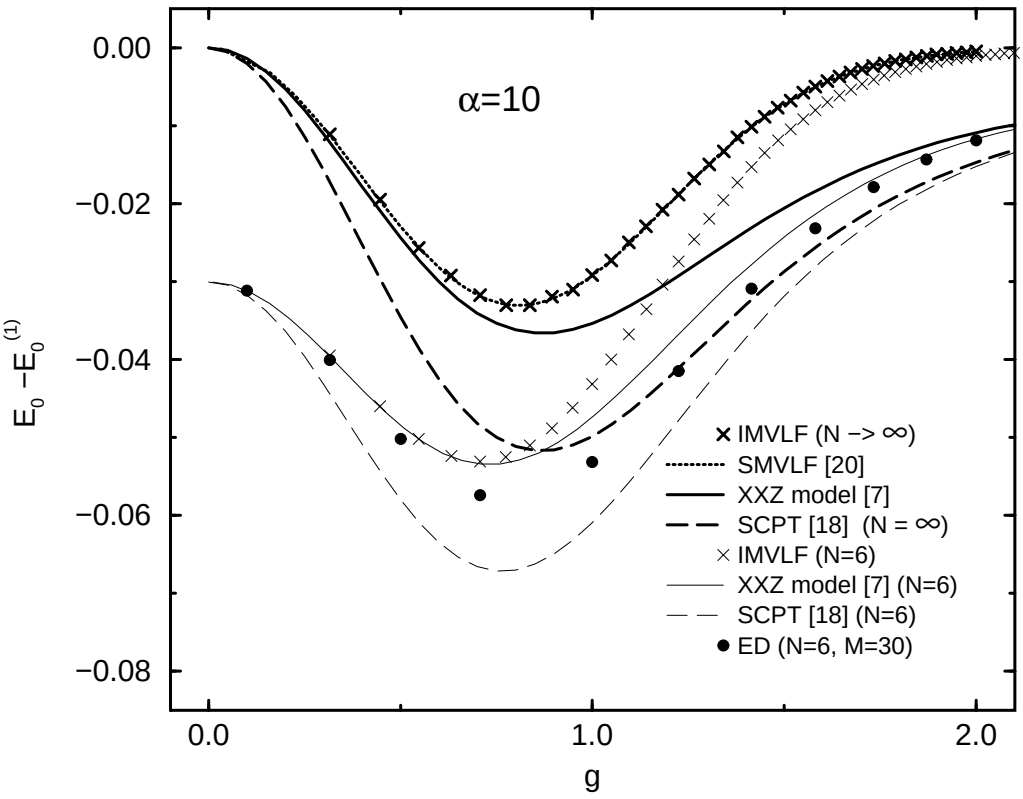
α=10
0.00
−0.02
−0.04
−0.06
−0.08
0.0
1.0
2.0
g
$E_0 - E_0^{(1)}$
IMVLF (N −> ∞)
SMVLF [20]
XXZ model [7]
SCPT [18] (N = ∞)
IMVLF (N=6)
XXZ model [7] (N=6)
SCPT [18] (N=6)
ED (N=6, M=30)

Figure 4:

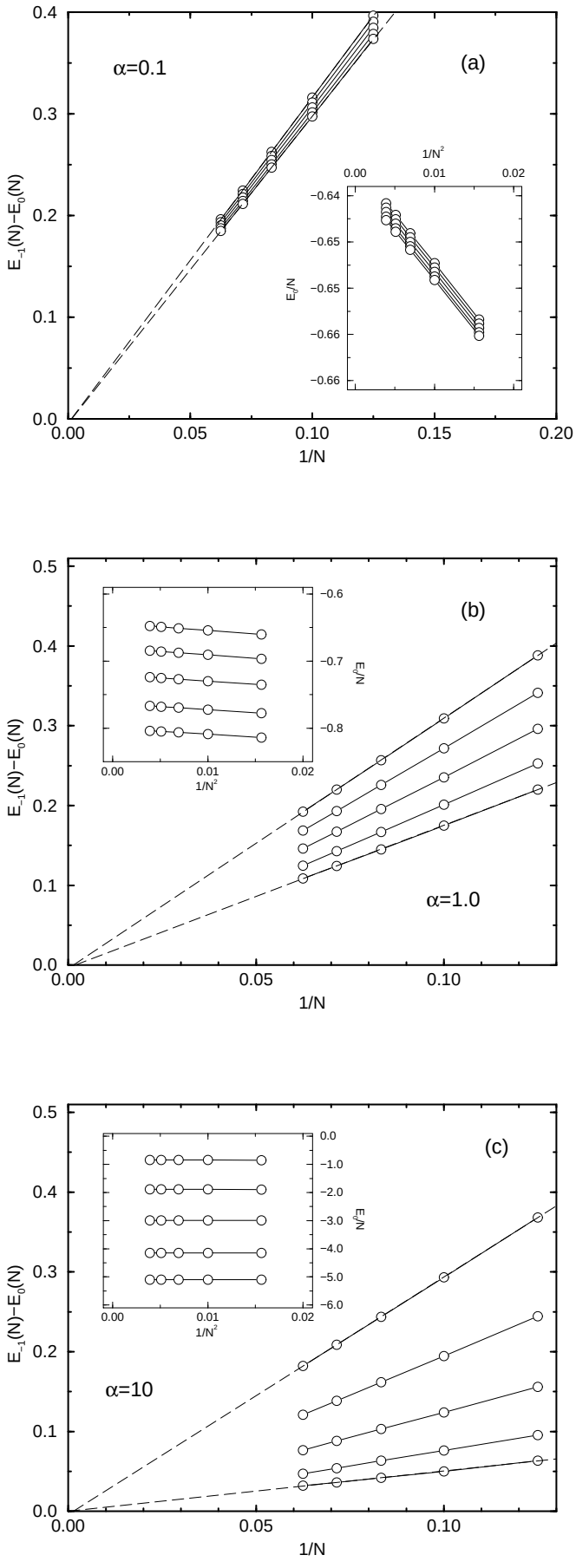

Figure 5:

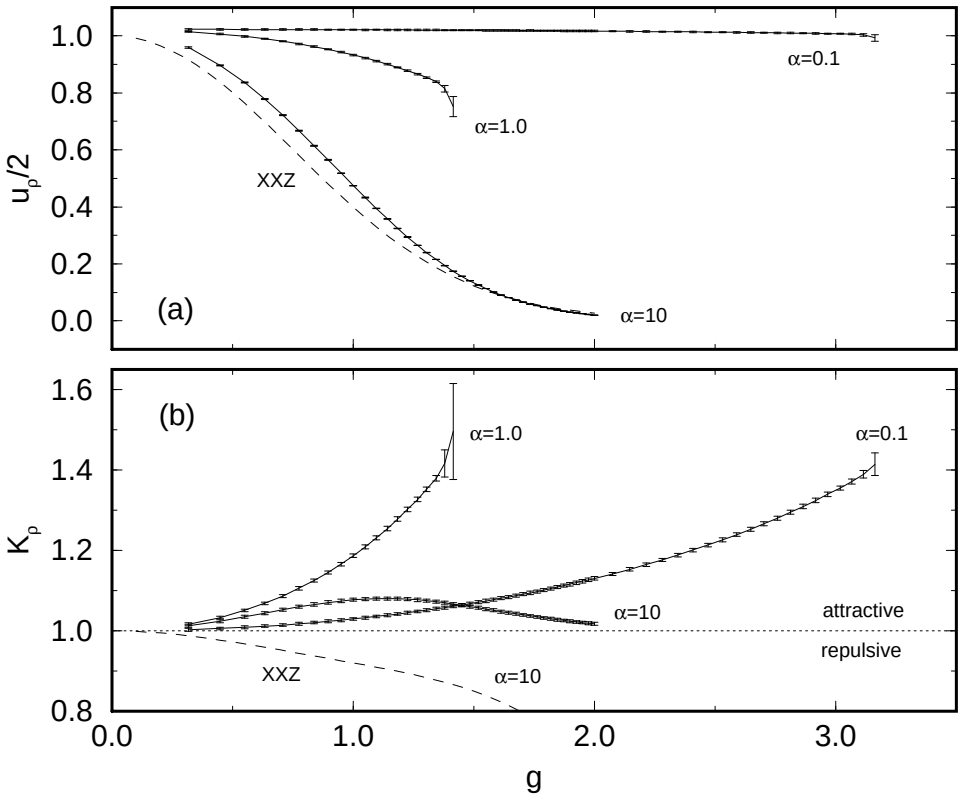
1.0
0.8
0.6
0.4
0.2
0.0
$u_\rho/2$
α=0.1
α=1.0
XXZ
α=10
(a)
1.6
1.4
1.2
1.0
0.8
K_ρ
(b)
α=1.0
α=0.1
α=10
attractive
repulsive
XXZ
α=10
0.0
1.0
2.0
3.0
g

Figure 6:

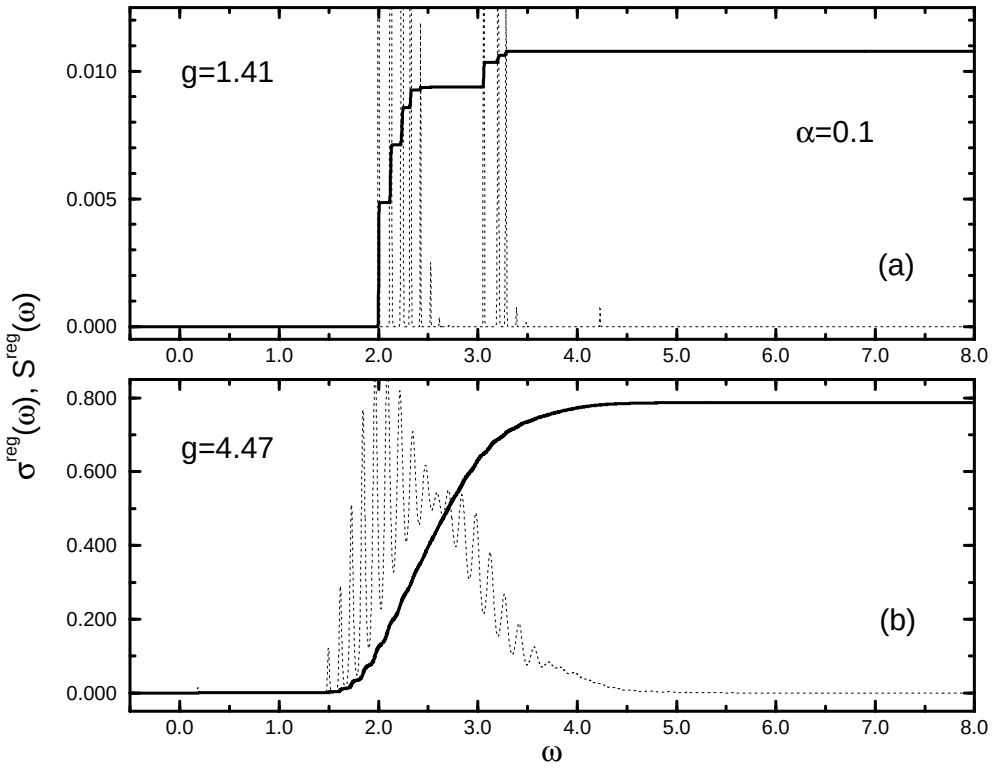
g=1.41
α=0.1
(a)
g=4.47
(b)
0.010
0.005
0.000
0.800
0.600
0.400
0.200
0.000
0.0
1.0
2.0
3.0
4.0
5.0
6.0
7.0
8.0
ω
σ^reg(ω), S^reg(ω)

Figure 7:

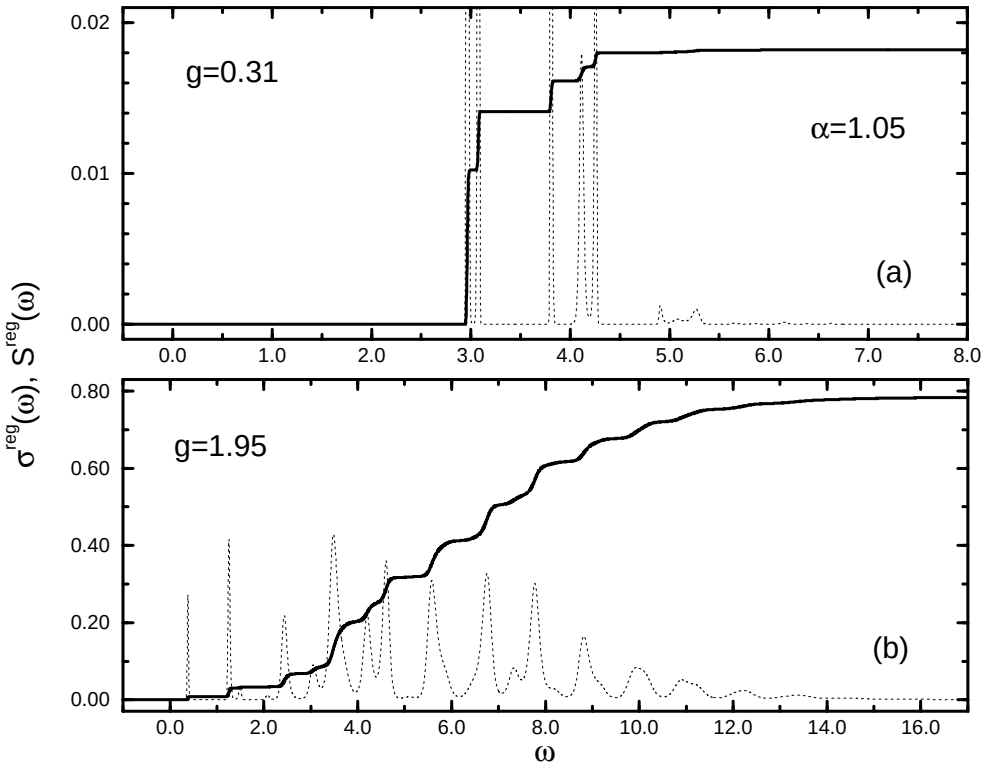
g=0.31
α=1.05
(a)
g=1.95
(b)
σ^reg(ω), S^reg(ω)
ω
0.02
0.01
0.00
0.80
0.60
0.40
0.20
0.00
0.0
1.0
2.0
3.0
4.0
5.0
6.0
7.0
8.0
0.0
2.0
4.0
6.0
8.0
10.0
12.0
14.0
16.0

Figure 8:

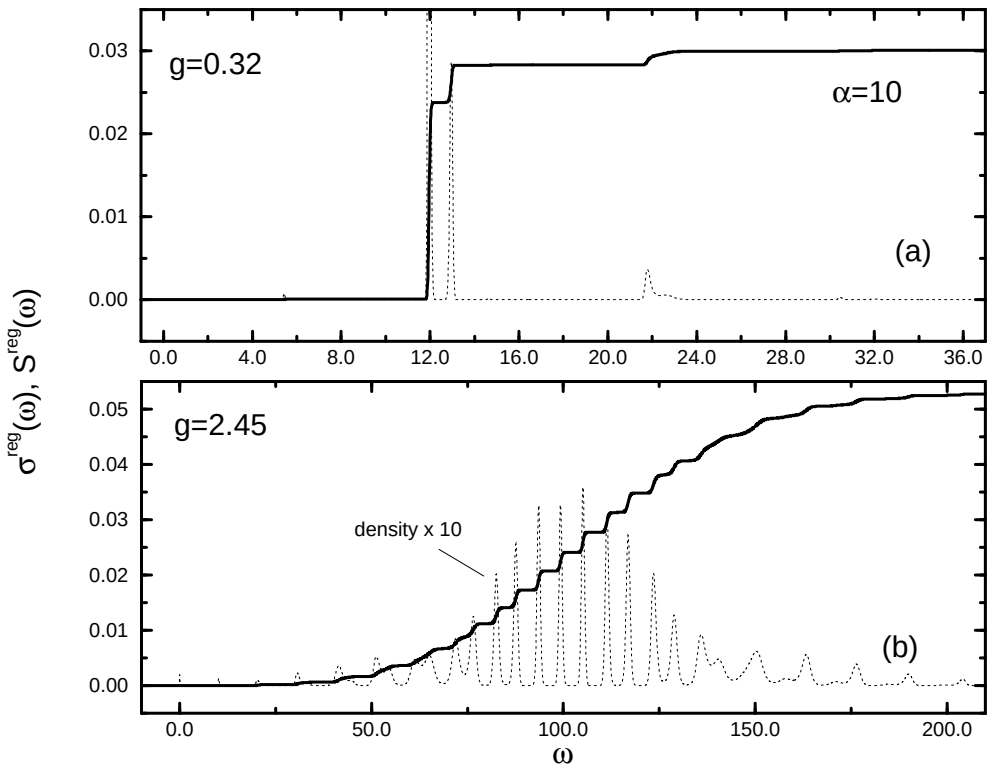
g=0.32
α=10
(a)
g=2.45
density x 10
(b)
σ^reg(ω), S^reg(ω)
ω
0.0
4.0
8.0
12.0
16.0
20.0
24.0
28.0
32.0
36.0
50.0
100.0
150.0
200.0
0.00
0.01
0.02
0.03
0.04
0.05

Figure 9:

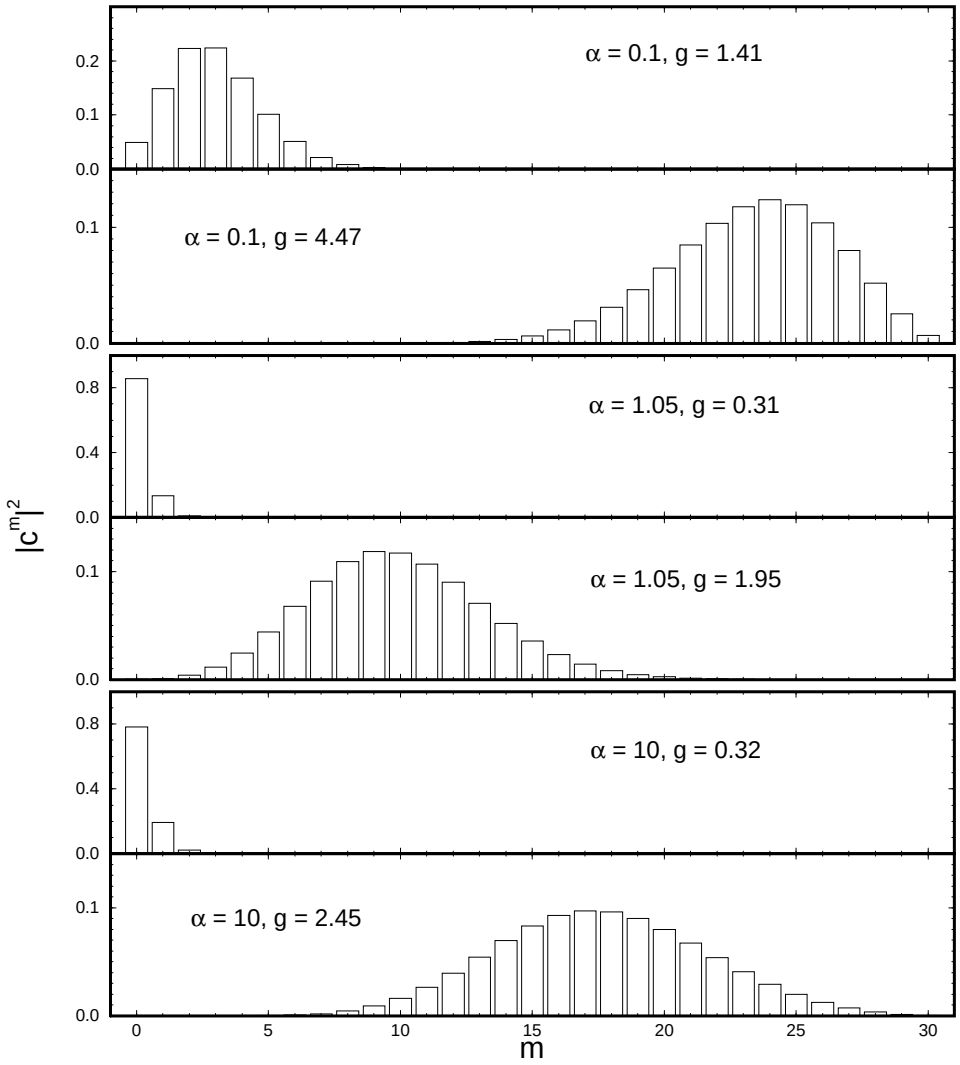
α = 0.1, g = 1.41
α = 0.1, g = 4.47
α = 1.05, g = 0.31
α = 1.05, g = 1.95
α = 10, g = 0.32
α = 10, g = 2.45
|c^m_l|^2
m
0.0
0.1
0.2
0.4
0.8
0
5
10
15
20
25
30